Title: Microrheology reveals microscale viscosity gradients in planktonic systems

Authors: Òscar Guadayol[1]*, Tania Mendonca[2], Mariona Segura-Noguera[1], Amanda J. Wright[2], Manlio Tassieri[3], Stuart Humphries[1]

Affiliations:

[1]School of Life Sciences, Joseph Banks Laboratories, University of Lincoln, Lincoln LN6 7DL, UK

[2] Optics and Photonics Research Group, Department of Electrical and Electronic Engineering, University of Nottingham, Nottingham, NG7 2RD, UK

[3] Division of Biomedical Engineering, James Watt School of Engineering, University of Glasgow, Glasgow G12 8LT, UK

Correspondence to: oscar@guadayol.cat

Abstract

Microbial activity in planktonic systems creates a dynamic and heterogeneous microscale seascape that harbours a diverse community of microorganisms and ecological interactions of global significance. Over recent decades a great deal of effort has been put into understanding this complex system, particularly focusing on the role of chemical patchiness, while overlooking a governing feature of microbial life affected by biological activity: viscosity. Here we use microrheological techniques to measure viscosity at length scales relevant to microorganisms. Our results reveal the viscous nature and the spatial extent of the phycosphere and show heterogeneity in viscosity at the microscale. Such heterogeneity affects the distribution of chemicals and microorganisms, with pervasive and profound implications for the functioning of the entire planktonic ecosystem.

One Sentence Summary: Microrheology measurements unveil the existence of viscous layers around phytoplankton cells and aggregates.

Main Text:

Planktonic microorganisms inhabit a microscale environment far more complex and dynamic than suspected even two decades ago. Microbial activity and diffusive transport generate chemical patchiness at length scales shorter than a few hundred micrometres, sustaining a diverse community of microalgae, protists, bacteria and viruses, with an intricate network of individual interactions and ecological processes of global significance (*1-3*). However, viscosity, a dominant feature of microbial life, has been overlooked in this emerging paradigm of microscale heterogeneity. Viscous forces govern directed motion and diffusion of microorganisms, particles and molecules in the very low Reynolds numbers regime experienced by microbes. This implies that small microorganisms may not directly experience turbulent flows, that mass transfer is ultimately governed by molecular diffusion and that biomechanical plans that work for large organisms become inefficient for microbes. Several studies [compiled in (*4*)] have reported increases in bulk viscosities of water, often higher than an order of magnitude, due to the presence of extracellular polymeric substances (EPS) exuded by phytoplankton and bacteria. In addition, intracellular viscosities can be up to two orders of magnitude higher than in water (*5*). However, very little is known about the role viscosity plays in shaping the heterogeneous microscale landscape.

Here, we hypothesize the existence of microscale viscosity gradients created by the same biological processes that generate chemical gradients around planktonic microorganisms (*2, 6*). We argue that the existence of microscale patchiness of viscosity will have fundamental

implications for the distribution of microorganisms and their resources, and therefore for the functioning of microbial planktonic ecosystems driving aquatic productivity globally.

To test our hypothesis, we characterized the variability in viscosity near live microorganisms, non-destructively and at micron length scales, by employing methodologies from the fast-evolving field of microrheology. In particular, we used microrheology with optical tweezers (MOT) and multiple particle tracking microrheology (MPTM). We investigated three distinct scenarios where we expected viscosity to be heterogeneous: (i) the phycosphere around healthy EPS-exuding phytoplankton cells (*6*); (ii) lysis events involving the release of cell content and (iii) algal cell aggregates.

To validate our hypothesis we first used MOT because its high spatiotemporal resolution allows the assessment of hydrodynamic effects near solid surfaces. We performed MOT measurements next to inert glass shards (mimicking siliceous diatom frustules) as a control and next to cells of *Chaetoceros affinis*, a diatom known to produce EPS (*7*) and to induce the formation of transparent exopolymer particles (TEP) and mucilages (*8*). Our results reveal that relative viscosities (defined as the ratio of local to background measured viscosities) are very variable near cell walls and tend to be higher than both measurements taken near glass shards and predictions from Faxén's laws (*9*), which describe hydrodynamic interactions near solid boundaries (Fig. 1A). Moreover, for measurements near cells, we also detected anisotropy in viscosity along the axes perpendicular and parallel to the cell wall, with both positive and negative departures from Faxén's laws (Fig. 1B), suggesting that EPS might be discreetly patterned in space. These observations are consistent with studies showing the presence of mucilaginous or gel-like structures around fixed bacteria and phytoplankton exuding EPS (*10-13*).

We next used MPTM to corroborate the MOT observations and to maximize the spatial coverage of the rheological measurements. Using MPTM we generated viscosity maps around plankton cells and aggregates, with a field of view (FoV) of 130×175 µm and a spatial resolution of 2x2 µm, which can be found in (*14*). The MPTM results for healthy *C. affinis* cells (Fig. 2) are in good agreement with those obtained from MOT. In 30 of the 41 cells analysed, we measured relative viscosities near the cell wall significantly higher than those predicted by Faxén's laws, but did not observe any significant increases around glass shards (Figs. 2, 3, S4 and S5, *14*). As with MOT, measured viscosity tends to decay nonlinearly away from the cell walls, suggesting exudation, diffusion and clustering of material from the cell. In all explored cases, viscosity values around diatom cells were highly variable, with areas showing enhanced values and others showing no noticeable increase. The thickness of the viscous layer around cells was also variable, ranging from 2 to 18 µm (Fig. 3).

To assess the prevalence of these viscous phycospheres, we next performed additional MPTM experiments on the diatoms *Cylindrotheca fusiformis* and *Skeletonema pseudocostatum*, on the dinoflagellates *Alexandrium minutum* and *Ostreopsis sp.*, and around colonies of *Phaeocystis globosa*, a haptophyte whose blooms are often associated with submesoscale (~1 km) increases in bulk-phase viscosity (*15*). We detected viscosity gradients near 45% of all cells analysed, and in all species except for *C. fusiformis* (Figs. 3, S4). The presence of a viscous phycosphere or its spatial extent, contrary to our expectations based on diffusive rates (*6*), did not correlate with cell size, while there was a high degree of intra- and interspecific variability. The spatial extent of the viscous phycosphere for the entire dataset appeared to be exponentially distributed (Fig. S4), with large viscospheres being more infrequent than small ones. Coefficients of spatial variability for viscosity in all experiments ranged from 8 to >2000 (Table S1), suggesting that viscosity patchiness can exist not only around cells and particles, but also in the fluid far from the cells, presumably due to the presence of colloids and mucus sheets (*1*). The highest relative viscosities we recorded (up to 80) were found inside the mucopolysaccharide matrix of *P. globosa* colonies (Fig S5).

The existence of a viscous layer around phytoplankton cells has profound implications beyond the physiological and ecological roles so far attributed to EPS (*16, 17*). A viscous phycosphere will fundamentally reshape a cell's physical environment. Exopolymers may allow microalgae to physically structure the phycosphere and modify flow fields (*18*). Critically, an increase in viscosity will reduce the rates of molecular diffusion, affecting nutrient uptake and exchange of infochemicals. It may also influence the distribution of bacteria around microalgae, not only because lower molecular diffusivities lead to steeper, longer-lived and easier to track gradients of chemoattractants, but also because viscosity-induced changes in swimming speed (*19*) may lead to changes in the distribution of bacteria (*20*). Thus, we propose EPS exudation may be an active strategy to recruit symbiotic bacteria to the phycosphere.

Viscous gradients may also be expected to develop when cells lyse, as intracellular viscosities can be several orders of magnitude higher than water (*5*). To test this hypothesis, we used MPTM to map viscosity around *C. affinis* cells before and after light induced lysis (*21*), as well as around dead *S. pseudocostatum*, *A. minutum* and *Ostreopsis sp.* cells. We detected increases in background viscosities after exposure to UV and bright light in some *C. affinis* samples, most likely because all cells within the FoV were lysed. Additionally, we observed localized patches of high viscosity around lysed cells (Fig. 2), as well as steep viscosity gradients around dead cells. Lysing and dead cells are a hotspot of microbial activity, as chemotactic bacteria swarm around them (*21*). Therefore, we would expect the same mechanisms at play in a viscous phycosphere to be magnified in a lysing cell, leading to a more efficient use of resources by chemotactic bacteria.

The last scenario we explored was of viscosity gradients generated by aggregates of phytoplankton. The formation of aggregates, TEP and marine snow is facilitated by EPS acting as a loose adhesive (*8*). We used MPTM to map relative viscosities inside and around shear-induced aggregates of the three diatom cultures. We observed increases in viscosity of more than an order of magnitude inside the aggregates (Fig. 4), with areas of enhanced viscosity largely overlapping areas stained by Calcofluor white (specific for β-d-glucopyranose polysaccharides). We regard these estimates as conservative because the spatial coverage of the MPTM maps inside the aggregates is limited by the capacity of the microspheres to penetrate the aggregates and by self-shading. Nonetheless, given the important role that aggregates play as hotspots for microbial activity and zooplankton foraging, and the importance of diffusive processes in sinking of porous particles in stratified fluids (*22*), our results could pave the route to new insights into processes influencing the biological carbon pump.

The implications of microscale viscosity gradients are grounded in theoretical physics and are pervasive, as viscosity impacts virtually all processes and interactions occurring in the microbial world. Increasing viscosity decreases the diffusivity of dissolved substances, small non-motile particles and organisms, and it slows motile plankton and sinking particles. Changes in viscosity will therefore not only affect the distribution of organisms and their resources, but may also slow down ecological rates, resulting in a cascade of effects at different ecological levels and scales. For example, increasing viscosity around osmotrophs will decrease nutrient uptake rates, potentially impacting primary and bacterial productivities. Similar reductions in encounter rates between predators (or viruses) and prey (or hosts) along with uncertain effects on the formation and sedimentation of aggregates, will ultimately influence the transfer of carbon across trophic levels and the strength of the biological carbon pump. Finally, given that viscosity often varies strongly with temperature, we must expect changes in viscosity in the context of global climate change, with the potential for unforeseen consequences for the carbon cycle and climate regulation (*23*). In summary, consideration of viscosity adds a new layer of complexity to the current paradigm of microscale heterogeneity. Our results provide a quantitative framework to explore how these ideas unfold from the microscale upwards.

References and Notes:

1. F. Azam, F. Malfatti, Microbial structuring of marine ecosystems. *Nature Reviews Microbiology* **5**, 782-791 (2007).
2. R. Stocker, Marine Microbes See a Sea of Gradients. *Science* **338**, 628-633 (2012).
3. M. A. Moran, The global ocean microbiome. *Science* **350**, aac8455 (2015).
4. I. R. Jenkinson, J. Sun, Rheological properties of natural waters with regard to plankton thin layers. A short review. *Journal of Marine Systems* **83**, 287-297 (2010).
5. D. Wirtz, Particle-Tracking Microrheology of Living Cells: Principles and Applications. *Annual Review of Biophysics* **38**, 301-326 (2009).
6. J. R. Seymour, S. A. Amin, J.-B. Raina, R. Stocker, Zooming in on the phycosphere: the ecological interface for phytoplankton–bacteria relationships. *Nature Microbiology* **2**, 17065 (2017).
7. S. Myklestad, O. Holm-Hansen, K. M. Vårum, B. E. Volcani, Rate of release of extracellular amino acids and carbohydrates from the marine diatom *Chaetoceros affinis*. *Journal of Plankton Research* **11**, 763-773 (1989).
8. T. Kiørboe, J. L. S. Hansen, Phytoplankton aggregate formation: observations of patterns and mechanisms of cell sticking and the significance of exopolymeric material. *Journal of Plankton Research* **15**, 993-1018 (1993).
9. H. Faxén, Der Widerstand gegen die Bewegung einer starren Kugel in einer zähen Flüssigkeit, die zwischen zwei parallelen ebenen Wänden eingeschlossen ist. *Annalen der Physik* **373**, 89-119 (1922).
10. F. Malfatti, T. J. Samo, F. Azam, High-resolution imaging of pelagic bacteria by Atomic Force Microscopy and implications for carbon cycling. *The ISME Journal* **4**, 427-439 (2010).
11. G. Pletikapić *et al.*, AFM imaging of extracellular polymer release by marine diatom *Cylindrotheca closterium* (Ehrenberg) Reiman & J.C. Lewin. *Journal of Molecular Recognition* **24**, 436-445 (2011).
12. E.-M. Zetsche, A. El Mallahi, F. J. R. Meysman, Digital holographic microscopy: a novel tool to study the morphology, physiology and ecology of diatoms. *Diatom Research* **31**, 1-16 (2016).
13. K. Li *et al.*, Capsular polysaccharide production from *Zunongwangia profunda* SM-A87 monitored at single cell level by atomic force microscopy. *Deep Sea Research Part II: Topical Studies in Oceanography* **155**, 44-49 (2018).
14. Ò. Guadayol, M. Segura-Noguera, S. Humphries. (figshare, 2020).
15. L. Seuront, D. Vincent, J. G. Mitchell, Biologically induced modification of seawater viscosity in the Eastern English Channel during a *Phaeocystis globosa* spring bloom. *Journal of Marine Systems* **61**, 133 (2006).
16. C. S. Reynolds, Variability in the provision and function of mucilage in phytoplankton: facultative responses to the environment. *Hydrobiologia* **578**, 37-45 (2007).
17. A. W. Decho, T. Gutierrez, Microbial Extracellular Polymeric Substances (EPSs) in Ocean Systems. *Frontiers in Microbiology* **8**, (2017).
18. T. Wyatt, M. R. d'Alcalà, Dissolved organic matter and planktonic engineering. *Production and fate of dissolved organic matter in the Mediterranean Sea*, 13–23 (2006).
19. V. A. Martinez *et al.*, Flagellated bacterial motility in polymer solutions. *Proc. Natl. Acad. Sci. U.S.A.* **111**, 17771-17776 (2014).
20. M. Demir, H. Salman, Bacterial Thermotaxis by Speed Modulation. *Biophysical Journal* **103**, 1683-1690 (2012).
21. S. Smriga, V. I. Fernandez, J. G. Mitchell, R. Stocker, Chemotaxis toward phytoplankton drives organic matter partitioning among marine bacteria. *Proc. Natl. Acad. Sci. U.S.A.*, 201512307 (2016).
22. K. Kindler, A. Khalili, R. Stocker, Diffusion-limited retention of porous particles at density interfaces. *Proc. Natl. Acad. Sci. U.S.A.* **107**, 22163-22168 (2010).

23. J. Taucher, L. T. Bach, U. Riebesell, A. Oschlies, The viscosity effect on marine particle flux: A climate relevant feedback mechanism. *Global Biogeochemical Cycles* **28**, 415-422 (2014).
24. Ò. Guadayol. (2020), pp. 'micro-viscomaps' is a set of matlab scripts that uses a Multiple Particle Tracking microrhology (MPTM) approach to generate maps of viscosity from a video of microspheres displaying Brownian motion.
25. R. R. L. Guillard, J. H. Ryther, Studies of marine planktonic diatoms: i. *Cyclotella nana* Hustedt, and *Detonula confervacea* (cleve) gran. *Canadian Journal of Microbiology* **8**, 229-239 (1962).
26. R. R. L. Guillard, P. E. Hargraves, *Stichochrysis immobilis* is a diatom, not a chrysophyte. *Phycologia* **32**, 234-236 (1993).
27. A. L. Shanks, E. W. Edmondson, Laboratory-made artificial marine snow: a biological model of the real thing. *Marine Biology* **101**, 463-470 (1989).
28. A. Yao, M. Tassieri, M. Padgett, J. Cooper, Microrheology with optical tweezers. *Lab on a Chip* **9**, 2568-2575 (2009).
29. F. Watts *et al.*, Investigating the micro-rheology of the vitreous humor using an optically trapped local probe. *Journal of Optics* **16**, 015301 (2013).
30. M. Tassieri *et al.*, Microrheology with Optical Tweezers: Measuring the relative viscosity of solutions ‘ at a glance ’. *Scientific Reports* **5**, 1-6 (2015).
31. M. Tassieri, Microrheology with optical tweezers: peaks & troughs. *Current Opinion in Colloid & Interface Science* **43**, 39-51 (2019).
32. S. Keen, J. Leach, G. Gibson, M. J. Padgett, Comparison of a high-speed camera and a quadrant detector for measuring displacements in optical tweezers. *Journal of Optics A: Pure and Applied Optics* **9**, S264–S266 (2007).
33. M. P. Lee, G. M. Gibson, D. Phillips, M. J. Padgett, M. Tassieri, Dynamic stereo microscopy for studying particle sedimentation. *Optics Express* **22**, 4671-4677 (2014).
34. J. Leach *et al.*, Comparison of Faxén's correction for a microsphere translating or rotating near a surface. *Physical Review E* **79**, 026301 (2009).
35. E. M. Furst, T. M. Squires, *Microrheology*. (Oxford University Press, Oxford, New York, 2017), pp. 480.
36. M. H. Sharqawy, J. H. L. V, S. M. Zubair, Thermophysical properties of seawater: a review of existing correlations and data. *Desalination and Water Treatment* **16**, 354-380 (2010).
37. Z. Qu, F. Z. Temel, R. Henderikx, K. S. Breuer, Changes in the flagellar bundling time account for variations in swimming behavior of flagellated bacteria in viscous media. *Proc. Natl. Acad. Sci. U.S.A.* **115**, 1707-1712 (2018).
38. B. S. McSwain, R. L. Irvine, M. Hausner, P. A. Wilderer, Composition and Distribution of Extracellular Polymeric Substances in Aerobic Flocs and Granular Sludge. *Applied and Environmental Microbiology* **71**, 1051-1057 (2005).
39. M. Pan, L. Zhu, L. Chen, Y. Qiu, J. Wang, Detection Techniques for Extracellular Polymeric Substances in Biofilms: A Review. *BioResources* **11**, 8092-8115 (2016).
40. A. L. Alldredge, M. W. Silver, Characteristics, dynamics and significance of marine snow. *Progress in Oceanography* **20**, 41-82 (1988).

Acknowledgements: We thank E. Berdalet for providing *Ostreopsis sp.* and S. Vaidyanathan for providing *C. fusiformis*. **Funding:** This research was funded by a Gordon and Betty Moore Foundation Marine Microbiology Initiative award grant 6852 to S.H. and O.G.. O.G.. M.T., A.W. and T.M .acknowledge support through EPSRC grant (EP/R035067/1, EP/R035563/1, and EP/R035156/1). **Author contributions**: O.G. and S.H. designed the study. T.M. developed the methodology and performed the experiments for MOT. M.T. developed the software for MOT analysis. O.G. developed the methodology and software for MPTM. O.G. and M.S.-N. performed the MPTM experiments. A.J.W. and M.T. provided guidance on the use and significance of microrheology. O.G and T.M wrote the paper. All the authors discussed the results and commented on the manuscript. **Competing interests**: Authors declare no competing interests. **Data and materials availability:** All MPTM viscosity maps have been deposited in figshare (*14*), as well as the code used for MPTM experiments and analysis (*24*). Any additional data that support the findings of this study are available from the corresponding author upon request.

Figures

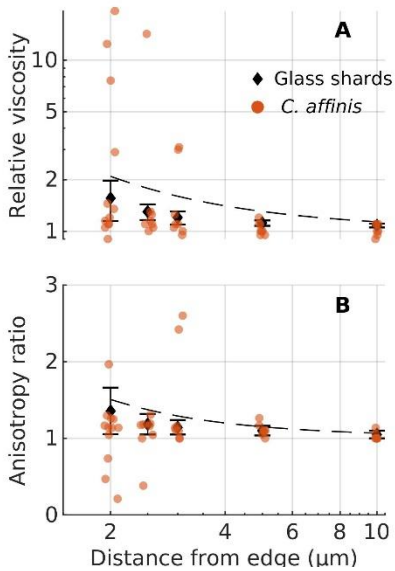

Fig. 1: MOT measurements of relative viscosity around *C. affinis* cells and glass shards in water as a function of distance from the object's boundary. Dashed black lines represent predictions from Faxén's laws (Eq. S2). (**A**) Relative viscosity in the direction perpendicular to the edge of the object. (**B**) Anisotropy in the measurements, given as the ratio of relative viscosities in the perpendicular direction to those in the parallel direction. An anisotropy ratio value of one represents isotropic conditions. Data has been jittered in the x axis by 0.1μm to facilitate visualization.

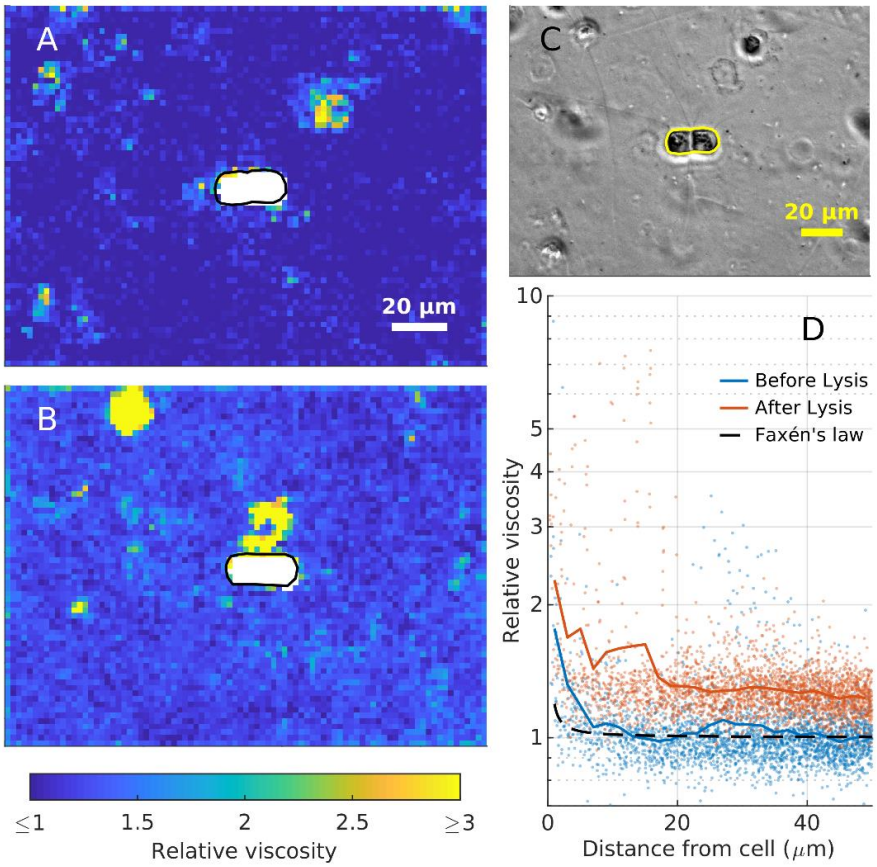

Fig. 2. Viscosity changes around a *C. affinis* cell before (**A**) and one hour after (**B**) Light-induced cell lysis. **A**, **B:** 2×2 µm MPTM viscosity maps. **C:** phase-contrast image at the start of the experiment. Cell boundaries are drawn in black in A and B, and yellow in C. **D:** viscosity estimates against the minimum distance to the boundary of the cell before (blue) and after (red) the lysis. Coloured lines are a moving average with a 2µm window. Dashed black line represents the prediction from Faxén's laws (Eq. S2).

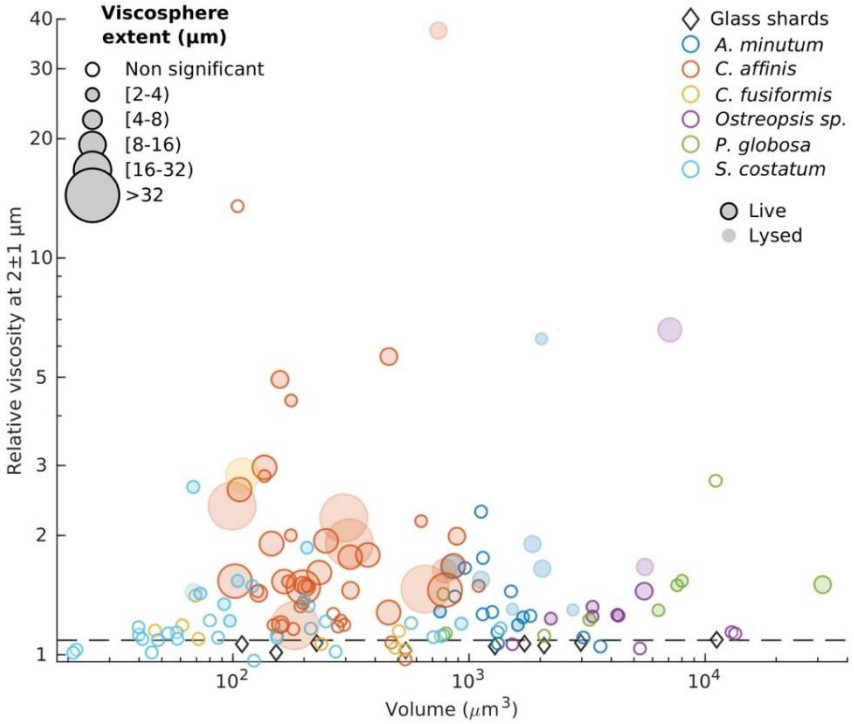

Fig. 3. Average relative viscosities 2±1 µm away from the cells in relation to the cells volume. The diameter of the symbols is proportional to the extent of the viscous phycosphere. Horizontal dashed line is the prediction from Faxén's laws (Eq. S2).

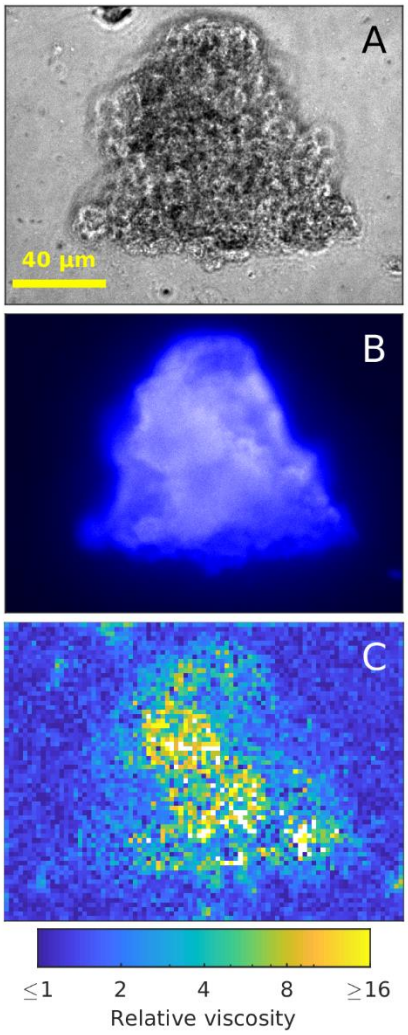

Fig. 4. Viscosity measurements inside and around a *C. affinis* aggregate. **A**. Phase contrast image. **B** CFW staining for polysaccharides. **C** 2×2 µm viscosity map obtained with MPTM. White pixels are areas with too few microsphere tracks to provide a reliable estimate.

Supplementary material

Material and Methods

Figures. S1-S7

Table S1

References (25-40)

Materials and Methods

Phytoplankton species and cultures. Formation of aggregates.

Growth conditions. We performed our experiments on the diatoms *Chaetoceros affinis* (CCAP 1010/27), *Cylindrotheca fusiformis* (CCAP 1017/2) and *Skeletonema pseudocostatum* (CCAP 1077/7), the dinoflagellates *Alexandrium minutum* (CCAP 1119/15) and *Ostreopsis sp*. (OOPM17 spp), and the haptophyte *Phaeocystis globosa* (strains K-1321 and K-1323, Norwegian Culture Collection of Algae). Diatoms were grown on f/2 + Si medium (*25*) in 33.5g/L artificial sea water (ASW, Aquarium Systems Instant Ocean Salt). *A. minutum* and *P. globosa* K-1323 were grown on L1 medium (*26*) in 30g/L ASW. *P. globosa* K-1321 was grown on TL medium (Norwegian Culture Collection of Algae) in 30g/L ASW. All species, except *Ostreopsis* sp., were grown at 19 degrees Celsius without shaking in an algae incubator (Algaetron AG 230, Photon Systems Instruments, Drasov, Czech Republic) in a 12:12h illumination cycle, with a light intensity of 100µE for diatoms and 90 µE for *A. minutum* and *P. globosa*. *Ostreopsis* sp. was grown with L1 medium in 38.5 g/L ASW and kept at lab temperature (20ºC) at the windowsill to ensure it received enough illumination. Cultures were not axenic and there were plenty of bacteria around. To ensure few bacteria were present, experiments were carried out less than two weeks after culture refreshment.

Aggregates of cells were formed from *C. affinis, C. fusiformis* and *S. pseudocostatum* cultures by incubating newly refreshed monocultures on a roller table (*27*). The roller was on the windowsill with natural light conditions at 20ºC. Within a few hours, aggregates were visible. Individual aggregates were collected very gently with a capillary tube to minimize disruption and prepared for the passive microrheological analysis using the same protocol than for phytoplankton below.

Optical trapping microrheology (MOT)

Microrheology with optical tweezers (MOT) uses single, optically trapped microspheres as probes for measuring the viscoelastic properties of the material surrounding them. Each microsphere is held by a tightly focused laser beam and can be manipulated in 3D space, allowing it to be placed at specific locations around an object of interest (e.g. a phytoplankton cell).

A microsphere confined within an optical trap will move with amplitudes on the nanometre scale due to the Brownian motion of the molecules in the surrounding material. The time dependent mean-squared displacement (MSD) calculated from the residual motion of each trapped microsphere can be used to compute the linear viscoelastic properties of the fluid around it as well as the strength of the optical trap (*28-31*). Depending on the camera used, this motion can be recorded at fast frame rates (≥1 kHz), allowing a frequency range of viscosities to be measured. At relatively long times or low frequencies viscosity is constant over a wide range of frequencies. Relative viscosity (the ratio of measured viscosity to the viscosity of water) can be calculated within this plateau region of viscosity by plotting the Normalised Position Autocorrelation Function (NPAF) against time (*30*).

In this study MOT was performed with polystyrene microspheres (diameter = 2.12 µm; 19508-2 Polysciences, Inc) as optically trapped probes for measuring the viscoelasticity of the artificial sea water (f/2 + Si media) at specific positions around individual *C. affinis* cells. The phytoplankton culture was refreshed the day before each experiment. The microspheres were dispersed at a final concentration of 0.0001% v/v in a dilute (10% v/v) solution of the *C. affinis* culture in f/2 + Si. This solution was loaded into µ-slide 8 well glass-bottom coverslips (ibidi GmbH) and incubated for ~2 hours at room temperature. The coverslips were pre-coated with poly-L-lysine (Sigma Aldrich P4707) to immobilize the phytoplankton cells and to prevent them from being drawn into the optical trap. Control samples were prepared in the same coated µ-slide coverslips using inert glass shards (from crushed coverslips – Borosilicate glass, 0.17µm thickness; Thermo Fisher Scientific) suspended in distilled water and in f/2 + Si media.

The microspheres were trapped using a 1064 nm continuous wave laser (Ventus 1064, Laser Quantum Ltd., UK) with a laser power of <5mW at the sample, and a high numerical aperture (NA) objective lens (100x 1.3NA Nikon CFI Plan Fluor). The trap depth was kept constant at 10µm from the coverslip throughout the measurements while the lateral position was varied. Each measurement involved a different microsphere and phytoplankton cell due to the challenges of retaining the same microsphere and cell for each sequence of positions. Each trapped microsphere was imaged in wide-field transmission on an inverted microscope (Eclipse Ti, Nikon) using a fast CCD camera (DALSA Genie, Teledyne Technologies International Corp). The time-dependent MSD of the trapped microspheres were tracked in real time and in 2D across 200,000 frames recorded at a frame rate of 1 kHz using a bespoke LabVIEW (version 2013 32bit, National Instruments) VI (virtual instrument) (*32*). The relative viscosity of the media around the cells/glass shards was calculated from the tracked coordinates using a previously published LabVIEW VI (the executable is free to download together with the instructions from the following link: https://sites.google.com/site/manliotassieri/labview-codes). Care was taken to ensure that the angle of approach of the trapped bead to the edge of the glass/cell was 90° and when this was not possible an offset angle was introduced to the analysis. Any effect of the poly-L-lysine on viscosity was controlled for each coated µ-slide by normalizing the viscosities to the measurements of microspheres in distilled water (relative viscosity = 1).

Edge effects. A moving sphere experiences an increase in hydrodynamic drag γ at close proximities to a solid surface and since the drag coefficient γ is proportional to the dynamic viscosity η of the fluid, this effect translates into higher apparent viscosities. The increase in γ is approximated by Faxén's laws (*9*, *33*) and depends on the radius of the sphere, *a*, its distance from the surface, *s*, and the viscosity of the material in which the sphere is moving. Microspheres in an optical trap will display motion in a harmonic potential due to the Brownian motion of the molecules in the surrounding material. Faxén's effect experienced by a microsphere during its motion parallel to the surface is given by (*34*):

$$\gamma^{\parallel} = \frac{\gamma}{1 - (9/16)(a/s) + (1/8)/(a/s)^3} \qquad (S1)$$

where $\gamma^{\parallel}$ is the corrected hydrodynamic drag for a sphere parallel to the surface, γ is the expected hydrodynamic drag, which for a sphere is $\gamma = 6\,\pi\, a\, \eta$. Similarly, for the microsphere's motion perpendicular to the surface the Faxén coefficient is:

$$\gamma^{\perp} = \frac{\gamma}{1 - (9/8)(a/s) + (1/2)(a/s)^3} \qquad (S2)$$

where $\gamma^{\perp}$ is the corrected hydrodynamic drag for a sphere parallel to the surface.

We assessed anisotropy in viscosity as the ratio between the viscosities estimated from motions perpendicular to the solid boundary (of a cell or a glass shard) and the viscosities estimated from motions parallel to the solid boundary

Passive multiple particle tracking microrheology (MPTM)

To assess spatial variability in viscosity at the microscale, we used passive multiple particle tracking microrheology (*35*). Briefly, the sample of interest is seeded with fluorescent microspheres of known diameter and density. The microspheres are tracked under the microscope as they undergo Brownian motion. From the analyses of their trajectories, and given a known and constant temperature, it is possible to estimate the local viscosity of the fluid into which the microspheres are embedded. We partitioned the 2D field of view into squares of given length and estimated the average viscosity from the analysis of all the tracks registered within each square. This procedure allowed us to generate maps of viscosity with a resolution of 2µm, around individual phytoplankton cells as well as around and to certain extent within aggregates. All our maps have been published without any preselection in a figshare collection (*14*).

Sample preparation and visualization. To measure local viscosity, a 1mL sample of the culture of interest was seeded with 50µL of a solution of fluorescent polystyrene beads of 0.29µm diameter (Fluoresbrite® YG Carboxylate Microspheres, Polysciences Inc). The solution of microspheres was prepared diluting one drop (~40µL) of the commercial solution into 2mL of the artificial seawater used to prepare the microalgae media. A surfactant (Tween 20), was added to the solution at 0.3% to facilitate the disaggregation of microspheres. Then, the microspheres solution was mixed on a vortex and sonicated in a bath sonicator for 5 minutes. The density of the microspheres is 1.05g/mL compared to 1.024g/mL of ASW at 33.5 salinity at 20ºC. Under these conditions the microspheres would sediment at ~1nm s^{-1} (*35*). The final concentration of microspheres in the solution was 2 10^9 microspheres mL^{-1} and the volume fraction was $2 \cdot 10^{-5}$. From these values it is possible to calculate and average distance between microspheres of 9µm (*35*).

Specimens were prepared by pipetting 100-150µL of the sample with microspheres on a slide in between two coverslips. The sample was then topped with a coverslip, sealed with vaseline to suppress any drift and placed on an inverted epifluorescence microscope (Zeiss AxioVert A1 Fl) equipped with an LED source (CoolLED pE-300 white) and imaged at 400X magnification with a long-distance objective (ZeissLD Plan-Neofluor 40x/0.6NA Corr). Pictures and videos were taken with a CMOS camera (Hamammatsu ORCA Flash 2.0). The field of view was 131 by 175 µm and the depth of field was 1.45µm. To perform an analysis we selected cells or aggregates that were isolated and completely still. Once the particle was selected, the fluorescent illumination was switched on and several consecutive videos were taken at 30 frames per second. Intensity of light was set to a maximum of 5% to avoid heating the sample or eliciting any response by the phytoplankton or bacteria.

We have identified the following potential sources of error in our method: inaccuracy of the temperature control, mechanical vibrations in the sample, inclusion of the analyses of tracks of clusters of microspheres and imprecision in the detection of particles and the estimation of their centroids. The first two error sources were minimized by controlling temperature throughout the experiments with a temperature stage (PE100-ZAL System, Linkam Scientific Instruments Ltd., Tadworth, UK) and by placing the microscope on an active antivibration table (ScienceDesk, Thorlabs Inc. Newton, New Jersey, United States). Furthermore, microsphere aggregates and other particles larger than single microspheres are discarded by the particle detection code.

When developing this methodology, we observed that microspheres could occasionally attach to cells or aggregates and move together with them. When analysing the tracks from these microspheres we obtained estimates for viscosity that could be several orders of magnitude higher than that of water because they were diffusing at the same rate than the larger particle. To avoid this potential source of error, we used Polysine™ slides (Thermo Scientific™) and targeted only cells, aggregates and glass shards that had attached to the slide and were completely still. To ensure this we took phase-contrast pictures before and after the tracking and discarded any videos in which the cells or particles of interest had moved. We focused ~ 10 µm above the slide to avoid wall effects and to image only microspheres that were freely moving. Preliminary tests with the Polysine slides confirmed that any wall effects were below the precision of the method (see below) and that they were adequately captured by Faxén's laws (Fig S5). As with MOT, control samples with inert glass shards (from crushed coverslips – Borosilicate glass, 0.17µm thickness; Thermo Fisher Scientific) were prepared on Polysine slides.

Lysis of individual phytoplankton cells was induced by exposing them to UV and white light at the maximum intensity for approximately 10 minutes, following Smriga et al. (*21*). The field of illumination was narrowed to minimize effects on nearby cells. In the case of diatoms, the lysing procedure was deemed successful when motile bacteria started to aggregate around the cell (signalling release of material). To minimize hydrodynamic interactions of swimming bacteria with the microspheres, we waited until the cloud of bacteria had dissipated before starting the recordings, which could take at least 10 minutes but no more than an hour. In the case of

dinoflagellates, which are motile, we immobilized the cells by exposing them to UV and white light at the maximum intensity for a short period of time. Upon exposure to intense light *A. minutum* and *Ostreopsis sp*. cells would first loose the lateral flagellum and then the polar one. If the light was left on for longer, a 'blob' of material would be seen coming out of the cell.

Viscosity calculation. Although it is possible to extract the frequency-dependent viscoelastic properties of fluids by using MPTM, in this work we use it only to measure viscosity because the relatively low number of particle trajectories and their short lengths in our application made spectral analysis tenuous. The field of view was partitioned into 2 by 2 µm squares. For each individual microsphere track we computed the squared displacements with time lags τ between 1/30 and 5/30 seconds. The squared displacements were grouped into the partitions according to their mean centroid, and the ensemble *MSD*s were computed for each partition. The diffusivity *D* of the microspheres within each partition was calculated by least squares fitting the data to:

$$MSD(\tau) = 2dD\tau \qquad (S3)$$

where $d = 2$ is the dimensionality of the tracks. The average dynamic viscosity η for each position was then calculated from the Stokes-Einstein equation for diffusion of a spherical particle:

$$D = \frac{k_B T}{6\pi a \eta} \qquad (S4)$$

where k_B is the Boltzmann constant and T is the absolute temperature.

Background dynamic viscosities were calculated as the median of measured dynamic viscosities for the entire field of view. Relative viscosities in MPTM viscosity maps were calculated dividing the local dynamic viscosities by the background dynamic viscosities. Reported background relative viscosities are background dynamic viscosities divided by the ASW dynamic viscosity estimated using equations in (*36*).

The image acquisition and analysis were conducted with in-house Matlab code. The microsphere tracking used a Matlab code initially designed to track bacterial cells [58]. All the code, including the code used to estimate local viscosities and create the maps, is available online under an GPL 3.0 license (*24*).

Viscosity profiles. To characterize the decay in viscosity away from a particle, the boundary of the particle was first characterized manually on the image using the command *drawpolygon* (*drawcircle* in the case of spherical *P. globosa* colonies) from the Image Processing Toolbox in Matlab. For each 2×2µm partition, the distance to the particle was computed as the minimum Euclidean distance to any of the boundary vertices.

A conservative estimate of the minimum length of the viscosity gradient was calculated for each particle in the following way. Viscosities were grouped into 2 µm wide bins according to their minimal distance to the boundary of the particle of interest. For each group a non-parametric Wilcoxon signed rank right-sided test was conducted with a 5% significance threshold to assess whether median viscosity was higher than the value predicted by Faxén's laws. To minimize the number of false positives, we used the Faxén's equation for movement perpendicular to the solid edge (eq. S2) which gives the highest value. The minimum length of the viscosity gradient was then estimated as the mid value of the bin immediately smaller than the first bin at which the median viscosity was significantly lower than the Faxén's prediction.

The volume of the cells was estimated assuming an ellipsoid shape where the two minor axes were assumed to be both equal to the width of the outlined cell boundary, while the major axis was equal to the length.

Method calibration and uncertainty. To quantify uncertainty, we first checked whether our method was systematically biased. We performed a series of microrheological experiments on ASW with a salinity of 33.5 at a range of different temperatures, from 5ºC to 35ºC, and

compared the results with the predictions from empirical equations for seawater (*36*). The slope of the least squares linear regression model is not significantly different from unity (Fig S6, *T*-test: $t(7) = 1.098$, $p = 0.309$), although our estimates were systematically higher than the theoretical prediction. We calculated this bias to be 2.4 10^{-4} (kg m^{-1} s^{-1}). In all subsequent calculations we subtracted this bias from our estimate for the dynamic viscosity.

We further tested our method outside the limited range achievable through changing temperature by comparing it against bulk measurements performed with a cone-plate rotational viscometer (DV2T Brookfield). We prepared a series of solutions of increased viscosity adding Ficoll 70, a highly stable, long chain synthetic polymer of fructose, to water. Aqueous solutions of Ficoll are Newtonian at the range of concentrations used in our study (*37*). Ficoll solutions were prepared by dissolving the polymer in ultrapure water and kept in a shaker rotating at 200RPM overnight. The results, after accounting for the bias with theoretical estimates, lie on a 1:1 slope for the entirety of the range (Fig S6).

We evaluated the precision of viscosity estimates in 2×2 µm square by calculating the bootstrap coefficient of variation (*CV*) from the seawater and Ficoll experiments outlined above. We estimated the unbiased *CV* as:

$$CV = \left(1 + \frac{1}{4N}\right)\frac{s}{m} \qquad (S5)$$

Where N is the number of tracks within a 2×2 µm square and s and m are the sample standard deviation and mean, respectively. The precision of viscosity estimates decreases nonlinearly with the number of tracks registered in a bin and does not depend on the viscosity (Fig. S7). In subsequent analyses, we used a minimum threshold of 20 tracks per bin to accept the viscosity estimate for any particular bin. This ensured a good coverage with a maximum *CV* of 20%. It should be noted that in most pixels the actual *CV* was much lower than 20%, as the average number of tracks was usually much higher than 20.

Exopolymer staining. Simultaneously with the MPTM of aggregates we assayed staining of the sample with several labels commonly used to visualize different EPS components in biofilms and flocs (*38, 39*). Explicitly, we tested i) Alcian blue (Sigma-Aldrich A5268), which is specific for negatively charged polysaccharides commonly used to dye transparent exopolymer particles (*40*), ii) FilmTrace SYPRO Ruby (TermoFisher Scientific F10318), which labels most proteins, iii) SYBR Green I, which labels nucleic acids, iv) Concanavalin A-Tetramethylrhodamine conjugate (Con A, Invitrogen™ C860), which labels α-d-Glucose and α-d-mannose, and v) Calcofluor white M2R (CFW, Sigma-Aldrich 18909), which labels β-d-glucopyranose polysaccharides. Alcian blue revealed an intricate network of polysaccharides within our samples, but we did not use it alongside MPTM because it precipitates in the presence of salts, creating a rigid matrix that alters the rheological properties of the fluid. Of the other stains, Concanavalin A and CFW produced the highest signal. In subsequent analyses of aggregates we used CFW.

Supplementary figures

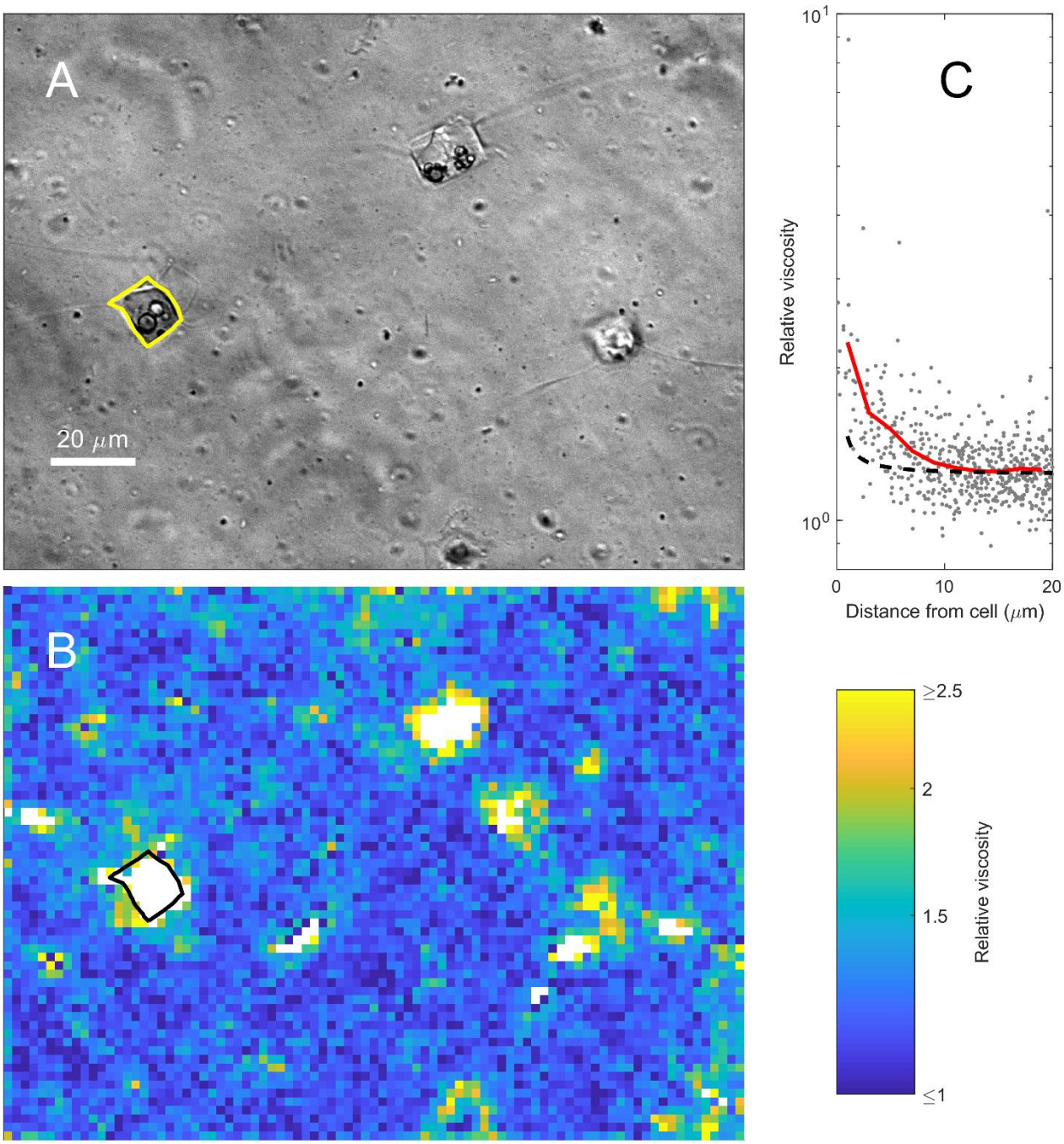

Fig. S1. Viscosity map and average profile around a healthy *C. affinis* cell. **A**: phase contrast image at the start of the experiment. **B**: map of viscosities estimated using MPTM. **C**: viscosity estimates against the minimum distance to the boundary of the cell. Red line in **C** is the moving average with a 2μm window. Boundary of the cell analysed is overlapped in yellow in **A** and in black in **B**.

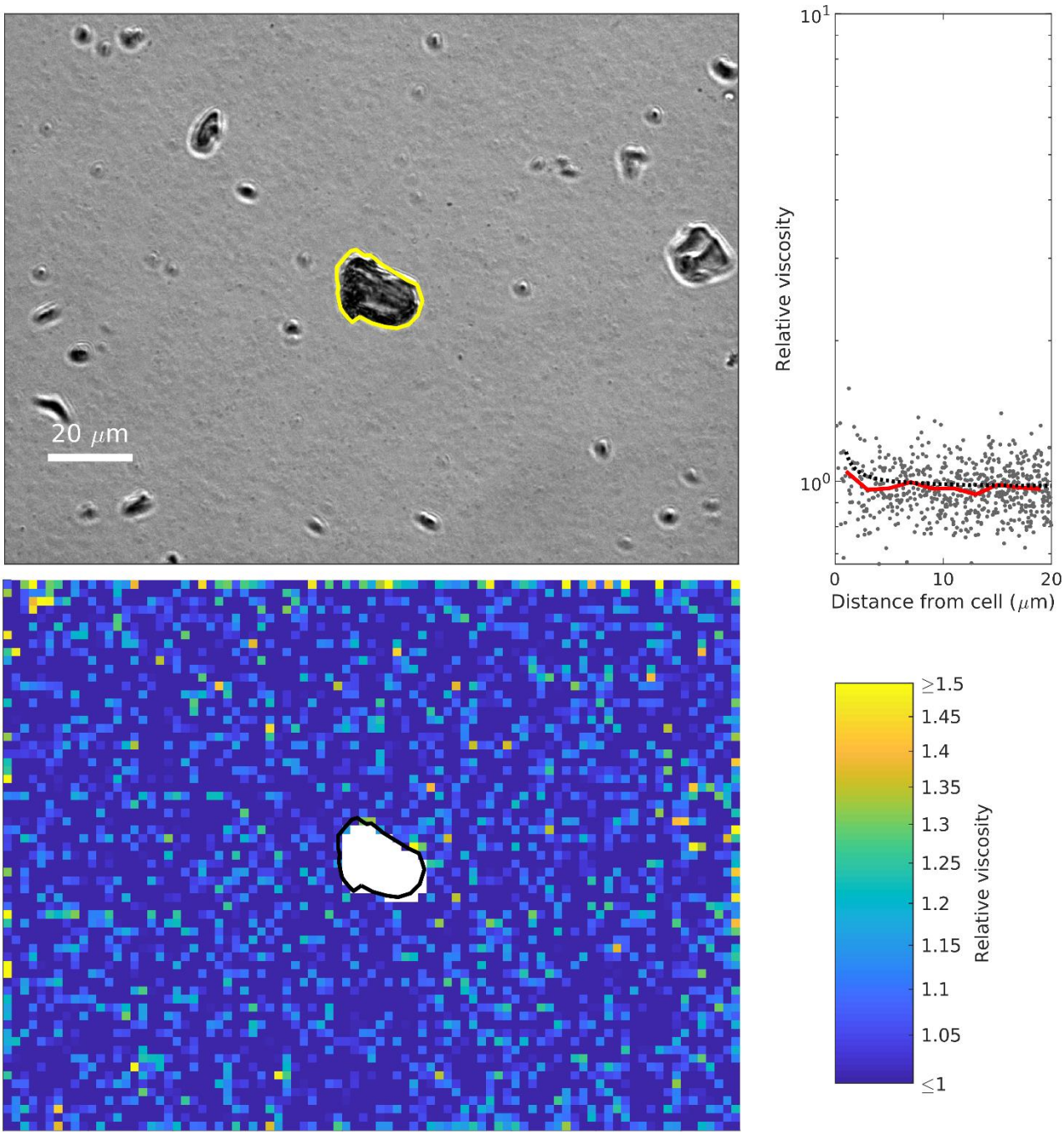

Fig. S2. Viscosity map and average profile around a glass shard. **A**: phase contrast image at the start of the experiment. **B**: map of viscosities estimated using MPTM. **C**: viscosity estimates against the minimum distance to the boundary of the shard. Red line in **C** is the moving average with a 2μm window. Boundary of the shard analysed is overlapped in yellow in **A** and in black in **B**.

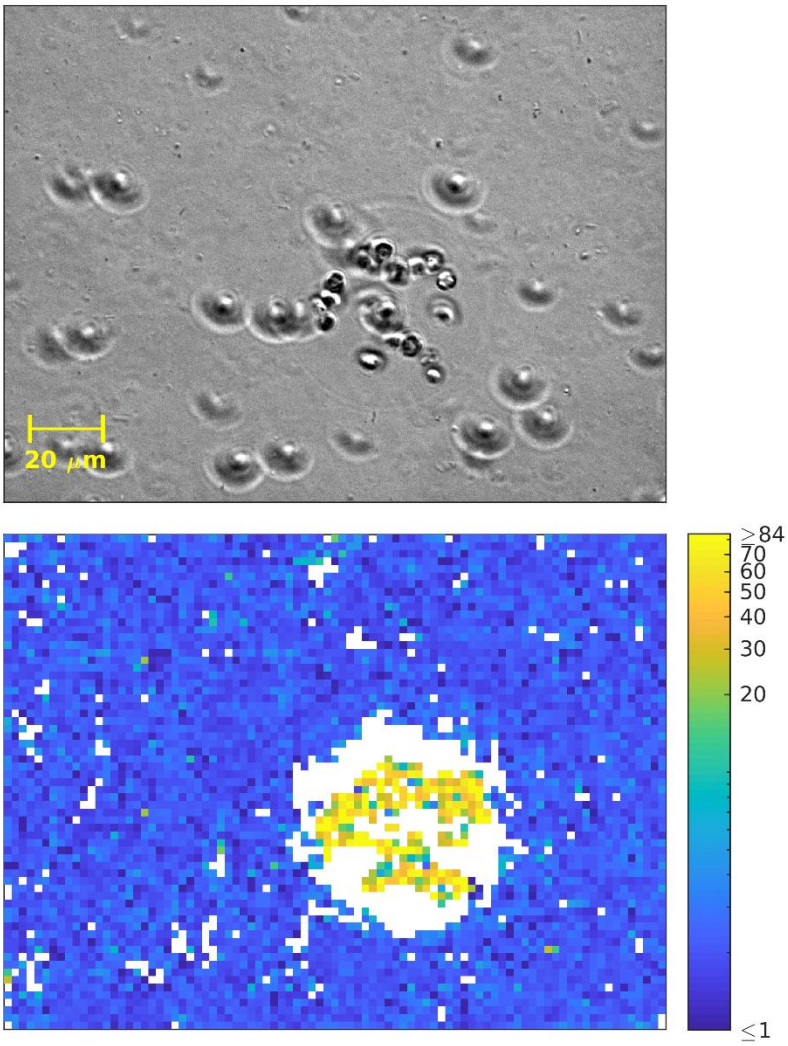

535 **Fig. S3**. Viscosity map of a *P. globosa* colony. **Top**: phase contrast image at the start of the experiment. **Bottom:** map of viscosities estimated using MPTM.

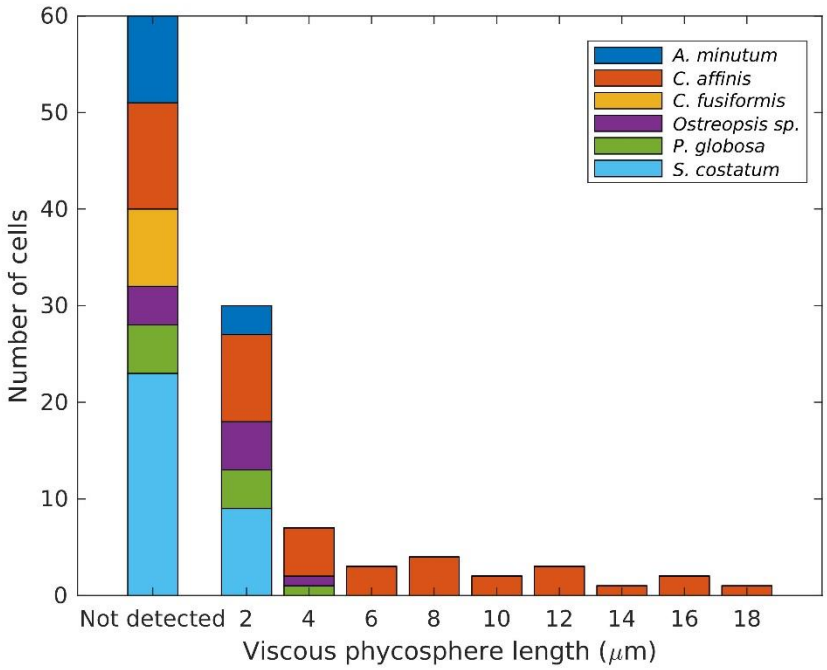

Fig. S4. Frequency distribution of the spatial extent of the viscous phycosphere among the phytoplankton cells analysed.

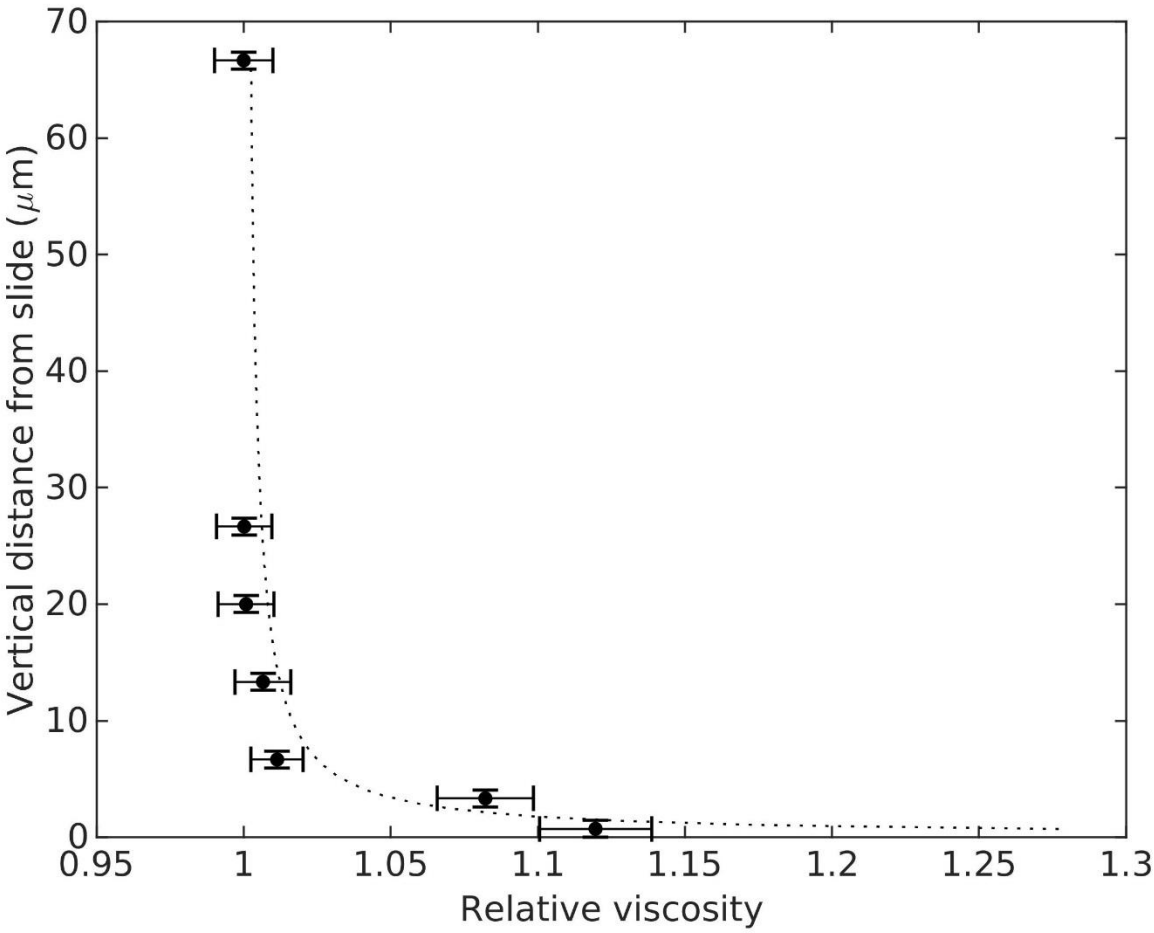

Fig. S5. Average relative viscosity of ASW with 33.5 salinity at 21ºC calculated with MPTM *vs* vertical distance from the slide. Horizontal bars are the standard errors. Vertical bars represent the depth of field. The dashed line is the apparent relative viscosity predicted by Faxén's law (eq. S1).

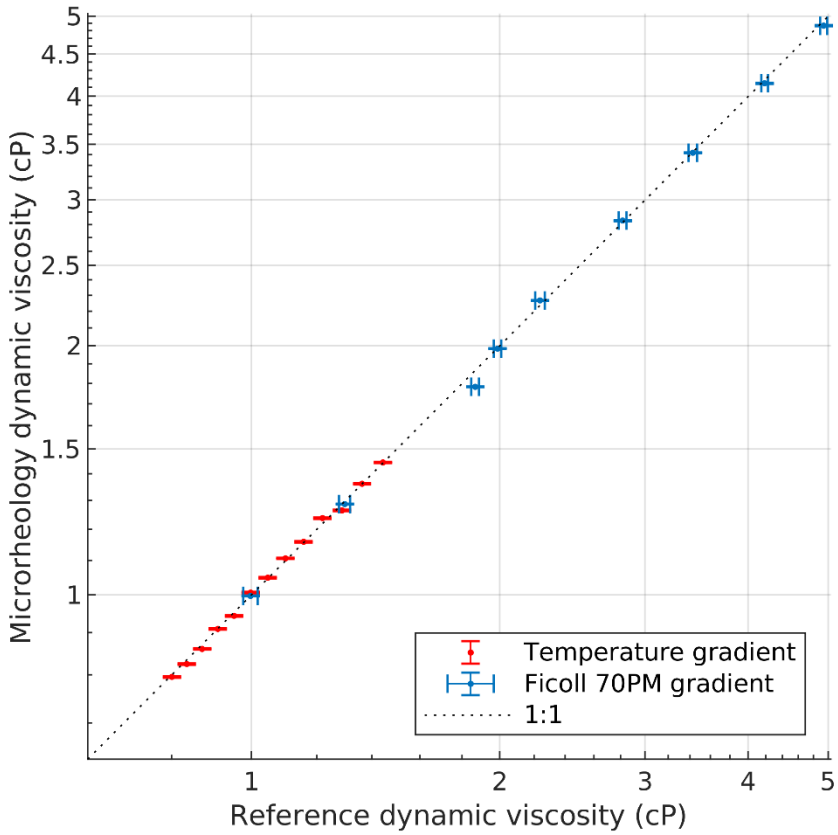

Fig. S6. Dynamic viscosities of artificial seawater at different temperatures (in red) and water solutions of Ficoll 70PM, estimated using MPTM against reference estimates. The reference viscosities for the temperature gradient were calculated using empirical equations in(*36*). The reference viscosity for the Ficoll gradient were measured with a DV2T Brookfield cone-plate viscometer. Vertical error bars show the standard errors. Horizontal error bars show the reported precision of the viscometer.

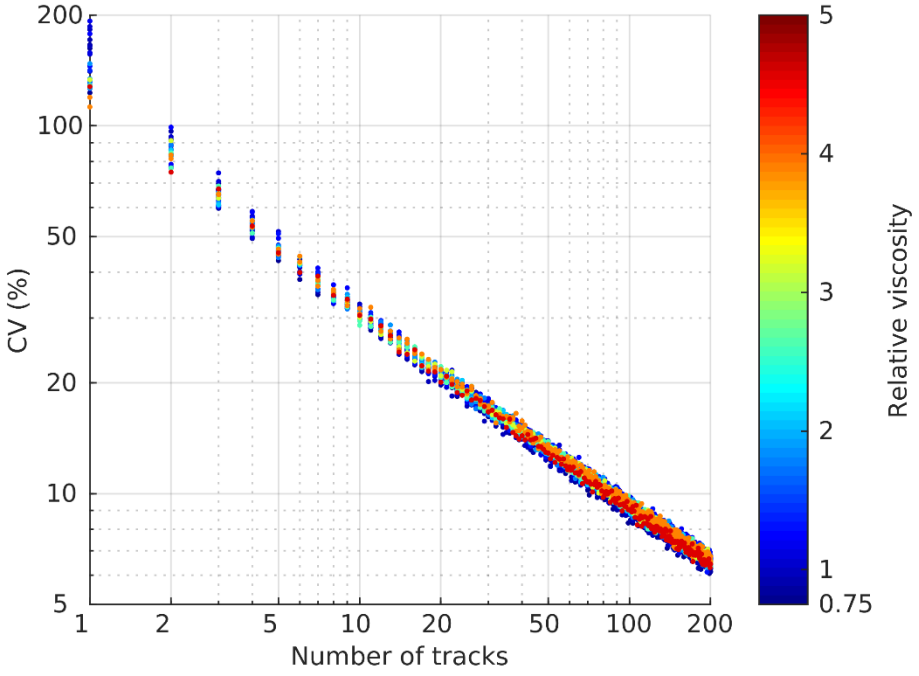

Fig. S7. Bootstrapped coefficient of variation against number of tracks per bin, which can be considered as the error for each pixel in the viscosity maps. Colour indicates the average viscosity of the sample used.

Supplementary table

Species	Bulk viscosity	MTPM		
		Number of experiments	Relative Viscosities	CV (%)
A. minutum	[1.00-1.02]	29	[0.7-1.2]	[16-559]
C. affinis	[1.00-1.93]	54	[1.0-3.2]	[15-1882]
C. fusiformis	[1.03-1.05]	12	[1.0-1.4]	[8-450]
Ostreopsis sp.	[1.01-1.06]	20	[1.0-4.1]	[11-830]
P. globosa	[1.01-1.08]	33	[1.0-6.8]	[9-2226]
(disrupted colonies)			[1.1-10.2]	[9-1390]
S. pseudocostatum	[1.00-1.01]	40	[1.0-1.3]	[14-68]

Table S1 Ranges of bulk-phase relative viscosities, measured with the cone and plate viscometer, and microscale relative viscosities measured with MPTM.